Effects of an industrial graphene grade and surface finishing on water and oxygen permeability, electrical conductivity, and mechanical properties of high-density polyethylene (HDPE) multilayered cast films.

José Carlos Ferreira Junior, Nima Moghimian, Giovanna Gutiérrez, Emna Helal, Abdellah Ajji, Guilherme Mariz de Oliveira Barra, Nicole R. Demarquette

PII: S2352-4928(22)00338-5

DOI: https://doi.org/10.1016/j.mtcomm.2022.103470

Reference: MTCOMM103470

To appear in: *Materials Today Communications*

Received date: 6 December 2021
Revised date: 14 March 2022
Accepted date: 29 March 2022

Please cite this article as: José Carlos Ferreira Junior, Nima Moghimian, Giovanna Gutiérrez, Emna Helal, Abdellah Ajji, Guilherme Mariz de Oliveira Barra and Nicole R. Demarquette, Effects of an industrial graphene grade and surface finishing on water and oxygen permeability, electrical conductivity, and mechanical properties of high-density polyethylene (HDPE) multilayered cast films., *Materials Today Communications,* (2021) doi:https://doi.org/10.1016/j.mtcomm.2022.103470

Effects of an industrial graphene grade and surface finishing on water and oxygen permeability, electrical conductivity, and mechanical properties of high-density polyethylene (HDPE) multilayered cast films.

José Carlos Ferreira Junior (1;2); Nima Moghimian (3); Giovanna Gutiérrez (3); Emna Helal (3); Abdellah Ajji (4); Guilherme Mariz de Oliveira Barra (2); Nicole R. Demarquette (1)

(1) École de Technologie Supérieure - Québec Canada,

(2) Federal University of Santa Catarina - Santa Catarina - Brazil,

(3) NanoXplore - Québec - Canada,

(4) École Polytechnique Montréal - Québec – Canada.

Abstract

Graphene-based composites are promising candidates to improve properties in flexible packaging to protect electronic devices. However, the literature hardly addresses the industrial scale requirements. In this context, high-density polyethylene (HDPE), a common packaging material, and an industrial grade graphene (G) were used to prepare multilayered composites by cast film coextrusion, a flexible-packaging-industry compatible technique. The effects of G content and surface finishing on HDPE films' properties were investigated. Experimental results showed that a maximum permeability reduction of 43% at 0.5 wt.% of G was achieved. Such result was associated with a good dispersion efficiency and with the filler's aspect ratio. However, as the concentration of G increased both barrier and mechanical properties worsened due to a poor dispersion of G within the composite. Additionally, it was found that surface finishing induced defects increasing permeability despite improvements in visible light transmittance and reduction of surface roughness. These defects can be successfully prevented using a proper design of layers during coextrusion. In summary, the present study showed the feasibility of G-based flexible packaging film applications at an industrial scale. The importance of G dispersion and of layer design to achieve improved barrier properties should be emphasized.

Keywords:
A. Polymer-matrix composites (PMCs); B. Microstructures; E. Extrusion.

1. Introduction

Flexible packaging ensures the protection of electronic devices against damaging effects such as those caused by moisture or electrostatic discharge. In this context, polymer-based composites are versatile

candidates for the flexible package industry allowing to tune key proprieties such as permeability. One of the main strategies used to control and reduce permeability in polymer-based composites is to increase the tortuous path [1] of the permeating species by dispersing a layered filler in a polymer matrix, improving its barrier effect. Dispersion is typically achieved by intercalation and exfoliation of the layered filler (e.g., clays, graphite and graphene) by means of solvents, polymer melt blending and/or filler modification [1,2]. At the research laboratory scale, polymer-based composites for barrier applications are usually obtained via solution processing. However, this technique is not suitable for cost-effective industrial applications, due to the large amounts of material required and scale up limitations. Thus, to promote the transfer of research findings on barrier properties to technological applications for flexible packaging, one should direct efforts towards processing techniques and materials suitable for an industrial scale, i.e., melt compounding of thermoplastics and large scale produced fillers. Still, there is little published research around the topic.

Concomitantly, carbonaceous based polymeric composites have gained increasing interest, as a research topic, over the last decade. Typically, fillers like carbon nanotubes, graphene, and their derivatives. These functional fillers enhance specific properties of polymeric composites, in particular, thermal conductivity, gas barrier, and electrical conductivity (antistatic and electromagnetic shielding effects), to name a few. In particular, graphene and its derivatives, can offer an interesting way to improve the performance of polymeric films used in the flexible packaging industry. For example, mechanical and electrical conductivity [3], barrier properties [4] among others [5].

To take advantages of the promising properties of graphene, great efforts were made recently to develop and optimize it's cost-effective powder production at industrial scale [6,7], suitable for melt compounding. The literature, concerning industrial graphene, however, mainly deals with materials of high structural variability [7], leading to large differences in terms of reported nomenclature and results [7,8]. Thus, for the sake of simplicity the performance evaluation of materials designated as graphene, graphene nanoplatelets, graphene microplates, or graphite microplates will, hereafter, referred to as graphene-based materials.

Some studies have therefore been conducted on graphene-based materials in polymeric composites and demonstrated that it is an effective way to reduce permeability. Permeability reductions of 18% to 45%

with a filler weight content up to 7 wt.% in different thermoplastic matrices, such as polypropylene [9], polyamide [10] and polycarbonate [11], compounded by means of extrusion, have been reported. However, in order to ensure lower cost and processability, as low as possible filler concentrations are usually recommended. Additionally, high filler concentrations adversely affect film transparency, coloring control, as well as, diminish barrier efficiency due to increased filler agglomeration [12]. Although some studies demonstrate the feasibility and potential use of graphene-based composites to improve barrier properties, two main drawbacks can be pointed out from literature analysis. First, the composites are usually produced by the compression molding technique and it is known that the barrier properties depend significantly on the manufacturing technique [13]. Thus, those results are not directly transferable [10] to commonly used fabrication techniques in the flexible packaging industry, like blown and cast films processes. Second, the most commonly used thermoplastic in the polymer packaging industry is polyethylene [14]. Polyethylene, however, is seldom used as polymeric matrix in studies of permeability involving graphene-based composites [1]. Therefore, in order to address some of the shortcomings found in literature regarding the processing technique and matrix on the composites performance, this study aims to extend the results to flexible packaging applications for electronics protection at the industrial scale based on cast film composites of high-density polyethylene (HDPE) and industrial grade graphene.

Herein, multilayered composite films of HDPE, the most common flexible packaging material, with an industrial (commercial) grade graphene (G) are produced in a coextrusion cast film line allowing layers design flexibility. The employed commercial graphene is produced through liquid phase exfoliation of graphite. This production route main advantages are low cost and environmental sustainability, by using water as processing medium [15]. Additionally, it has been shown this G to be of lower health risk than other fillers [16].

The two main investigated parameters in this study are the surface finish, to produce more homogenous film surfaces, and filler loading up to a maximum of 1 wt.% to reduce agglomeration and the negative impact in films transparency. The influence of those parameters on, the oxygen and water vapour permeability, electrical conductivity, and mechanical properties were investigated. Furthermore, a discussion

of the effect of filler agglomeration on these properties is presented. Finally, permeability and mechanical response are evaluated in light of theoretical models in order to validate and interpret the obtained results.

2. Experimental

2.1. Materials

The polymeric composite films were prepared using high density polyethylene-hexene copolymer pellets under the commercial name Formolene HB5502B (Formosa plastics, USA). The reported physical properties are a density of 0.955 g/cm^3 and melt flow index of 0.35 g/10 min (190 °C/2.16 kg). A commercial graphene grade was used in the form of master batch (MB) pellets composed of HDPE Formolene HB5502B and 40wt% of GrapheneBlack 3X (Nanoxplore Inc., Canada) [17] with an electrical conductivity of 1.2×10^{-2} S/cm measured with the four-point probe method. All materials were used as received and kindly supplied by Nanoxplore Inc. (Canada).

2.2. Methods

2.2.1. Film fabrication

Films of 8 layers were fabricated using a coextrusion cast line (LabTech engineering, Thailand) with four single screw extruders with a ratio length/diameter of 30 and equipped with Maddock mixing screws. The MB was diluted with HDPE to three different compositions, 0.1 wt.%, 0.5 wt.% and 1 wt.% of G directly in the single screw extruders (SSE). Those concentrations were kept the same for each one of the eight layers. Neat films were prepared for comparison with the composites. Temperatures from feeding zone to the metering zone were, 200 °C, 220 °C and 240 °C with a screw speed of 20 rpm for all extruders. The connection pipes from the extruders to die were set at 220°C and the flat die at 240 °C. A 300 mm flat die with a lip opening of 150 µm was used to achieve films with average thickness of 100 µm resulting in a draw ratio between 1.3 – 1.5 considering the final film thickness. The casting roll and die exit distance was set to less than 20 mm with parallel alignment to avoid melt sagging. Rolls were used in a vertical alignment position with chill rolls set to 90 °C to reduce surface defects and promote a more symmetrical microstructure [18].

To compare the effect of the surface finish on the films properties, a polishing roll was used to nip the samples with 0.2 MPa at 90 °C, resulting in a film with smooth surface. Those samples were identified as nipped (N) and compared against the reference group, without surface finishing and identified as non-nipped (NN).

2.3. Characterization

The transparency, morphology, barrier, mechanical and electrical properties of the obtained samples were characterized using different analytical techniques at room temperature. The measurements were performed in duplicate, on samples arbitrarily taken from the center of the fabricated films for each composition and surface finishing, unless otherwise stated. When relevant, the orientation in which the samples were tested is indicated by machine direction (MD) and transverse direction (TD) throughout the article.

The transparency of the produced films was estimated by evaluating the light transmittance in the visible range (340 – or to 1000 nm) of square shaped films with a side length of 50 mm using a UV-Vis Thermo Scientific SPECTRONIC 200.

The morphology of the samples was characterized by optical microscopy (OM), scanning electron microscopy (SEM), transmission electron microscopy (TEM) and atomic force microscopy (AFM).
The surface (top view) and cross section (MD) of the films (SI) were observed with an optical microscope in transmission mode (model Olympus BX51). The images were captured using an OptixCam Summit SK2-5.2X digital camera. Pictures of surface and cross section were taken at a 100- and 1000-times magnification respectively, both from at least 3 random areas. An automated approach was employed using the Image Processing Toolbox of MATLAB 2020a software to investigate the filler dispersion, alignment, and size. The main operations of the automated approach were: noise reduction, polymeric matrix background removal, particle identification and summation of the projected particles area within different focused regions of the same area under analysis. A conversion factor was applied to the identified particles based on the picture's pixel information and sample size through a micrometer calibration procedure in the microscope. The obtained data based on top view pictures were: average particle length size, D50, D90 and maximum particle

size, The average G particle thickness was obtained from the image processing of cross section pictures. To clarify, particle size in this context refers to the size (length or thickness) of the G agglomerate instead of the smallest constituent unit of a material. Samples were also observed with a SEM Hitachi MEB-3600-N at an accelerating voltage of 5kV and by TEM using a JEOL model JEM-2100F at 200 kV. In this case, films embedded in a mounting resin were prepared by ultra cryomicrotomy at -160ºC. These samples were analyzed in in the machine-transverse (M-T) plane to investigate G aspect ratio. The surface roughness of 10-mm samples (25 µm2 of analyzed area) was determined using a Bruker EnviroScope AFM in tapping mode. It was calculated by averaging the absolute values of the obtained profile.

The water permeability was evaluated in a MOCON AQUATRAN model 1 using an exposed area of 50 cm². The amount of water vapor transmitted across the films was determined at 37.8 °C in a saturated atmosphere (100% relative humidity). The duplicates were tested at the same time with 24 hours of conditioning before each measurement. The oxygen transmission rates were assessed using a MOCON OX-TRAN 2/21 ST equipment at 23 °C and 0% relative humidity with an exposed area of 100 cm² and 4 hours of conditioning. At least 4 measurements were done for each sample, and the reported permeability is given by averaging those measurements. Both water and oxygen permeability results were normalized by the films thickness obtained from 4 measurements with a micrometer screw gauge.

The crystallinity of the films was determined by DSC (PerkinElmer model Pyris 1) to evaluate its possible influence on oxygen and water permeability results. For that, a sample was taken from the center of the same films tested in permeability. The sample was encapsulated in an aluminum pan and analyzed in the range from 50°C to 200 °C at a heating rate of 10 °C/min. The percentage of crystallinity was determined according to Equation 1:

$$C_{\%} = \frac{\Delta H_m}{\Delta H_m^0} \cdot 100 \qquad \text{Equation 1}$$

Where, the ΔHm is experimental heat of fusion and ΔH0m is the enthalpy of fusion of a theoretical 100% crystalline HDPE, which was assumed to be 293 J/g based on literature [19].

The mechanical properties of the obtained films were obtained in tensile mode using an Instron ElectroPuls E3000 equipment with a load cell of 250 N at a 2 mm/sec rate. Samples in the machine direction

(MD) and transversal direction (TD) were cut from the produced films into rectangular shapes of 20 mm × 80 mm. They were fixed between pneumatic grips with the help of rubber pieces to avoid sample slippage.

Volume resistivity measurements (ρ) were conducted using the two-probe standard method with a Keithley 6517B electrometer and a Keithley 8009 test fixture. Volumetric conductivity (σ) values were obtained according to Equation 2:

$$\sigma = \frac{1}{\rho} = \frac{1}{\left(\frac{22.9V}{i \cdot t}\right)} \qquad \text{Equation 2}$$

A voltage V of 200 V was applied for 180 seconds followed by 180 seconds of discharge. The current i was taken as the average value after 60 seconds of the initial applied electrical potential. Thickness t was determined by averaging five values taken from random regions using a micrometer screw gauge.

3. Results and discussions

3.1. Surface roughness and light transmittance

The surface finishing and optical properties are important requirements in the flexible packaging industry since they can give the manufacturer the ability to display the product inside the packaging [13]. The average surface roughness (SR) of the samples, as well as the average peaks and valleys height are presented in Table 1. As expected, non-nipped (NN) sample present rougher surfaces when compared to the nipped (N) one. The restricted cooling and pressure imposed by the chill-rolls for the nipped samples result in a more homogeneously and smoother surface, with smaller peaks and valleys and lower variability among them. It can be also seen from Table 1 that the increase of G content also resulted in an increase of the SR of the surface finished films.

Table 1 – Average values of surface roughness (SR), peaks and valleys height.

Group	Filler weight Content (%)	Average SR (nm)	Average peak height (nm)	Average valley height (nm)
Nipped (N)	0	4.8±2.5	13.7±12.3	4.7±8.3
	0.1	7.1±7.8	23.1±13.2	16.3±15.6
	0.5	7.5±4.2	27.7±20.3	15.0±15.6
	1.0	8.5±2.3	19.0±13.7	8.7±9.7

Non-nipped (NN)	0	30.0±19.8	70.4±35.6	25.1±32.3
	0.1	29.3±27.0	61.9±29.0	17.4±31.4
	0.5	19.9±22.1	52.6±46.7	16.0±35.0
	1.0	23.1±34.6	80.8±58.7	108.7±91.3

The surface finish resulted in an increase ranging from 1.9 % to 49.6 % in light transmission for the neat HDPE. This transparency enhancement can be explained by the reduction of SR which results in a more homogenous surface decreasing light scattering effects at the surface. The introduction of graphene led to light transmission attenuation due to increased light scattering and absorption effects [20,21]. Further increase in G content led to a 99.8% reduction in transmittance at 1 wt.% compared to the neat N material. In contrast, a similar trend of decrease in transmittance and increase in SR was not observed for the NN composite films. This could be attributed to a high variation of SR of NN samples, as shown in Table 1. Interestingly, N 0.1 wt.% films exhibited higher light transmittance than the NN neat HDPE films. These results are in good agreement with the visual appearance of the composite films, with the N films being more transparent to the naked eye than the NN films.

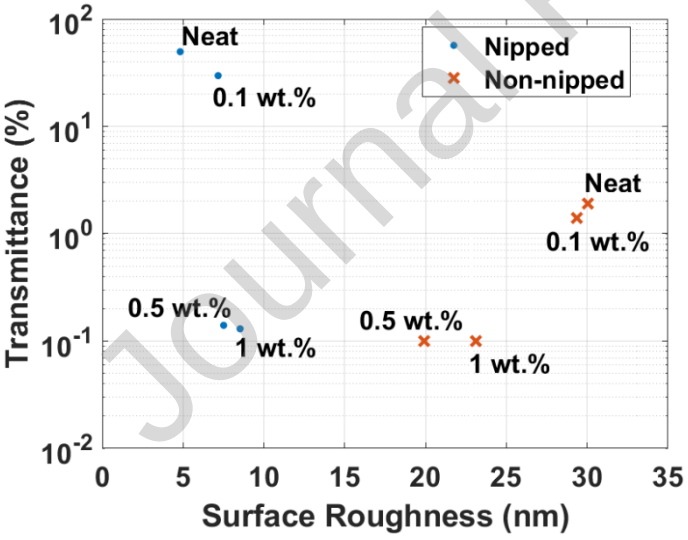

Figure 1

3.2. Filler average size, dispersion, alignment, and aspect ratio

Gas permeability performance of a composite material depends on the state of the dispersed phase inside the film. Taking that into account, optical microscopy (OM) was used as a fast tool to identify the

dispersion state of the fabricated films from top view and cross section. Both matrix and the G phase were easily distinguished in transmission mode due to the small amounts of G and the small film thickness (100 µm). Figure 2 depicts the top and cross section view images of a NN sample after image processing for the three evaluated graphene contents used for the quantification of the particles' parameters. The N samples presented similar results.

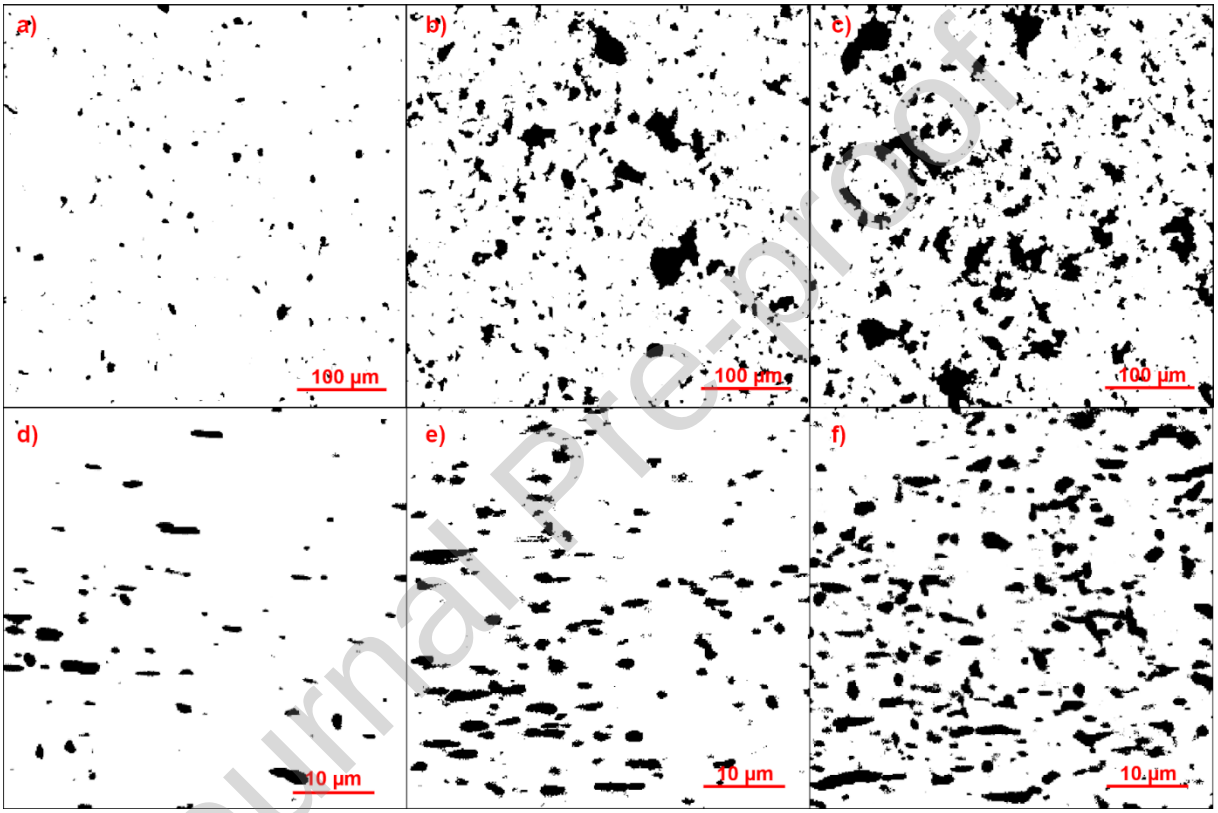

Figure 2

Good dispersion and distribution of graphene can be qualitatively observed in Figure 2. The graphene displays a platelet shape and preferential alignment parallel to the films surface, induced by the processing technique as presented in Fig.2 d)-f). Such alignment is desired and beneficial to reduce the composites permeability [2].

Table 2 summarizes the average graphene particle size, D50, D90 and maximum size in terms of length size of graphene agglomerates and average graphene agglomerate thickness measured for both studied groups (N and NN). Length and thickness are assumed based on the preferential alignment observed. For the same graphene content, both N and NN samples show a similar average size with half of the fillers being less

than 3 µm in length and similar distribution throughout the matrix. The increase in G content resulted in a higher number of larger agglomerates. This agglomeration effect is observed on the increase of the average G length, D90 and maximum particle size found in the matrix. The increase of G content is accompanied by an increase of graphene agglomerate thickness (Table 2) indicating that filler is indeed dispersed in the form of agglomerates. This observation suggests a reduction in extruder efficiency to deagglomerate the G at higher contents. Considering the analysis limitations of OM in observing smaller particles, a TEM analysis was carried out for the 0.5 wt. % G films in the machine-transverse (M-T) plane for both N and NN groups. The TEM images are depicted in Figure 3.

Table 2 – Summary of size measurements, average values, D50, D90, maximum size (Max.), average thickness, and aspect ratio of G agglomerates for nipped and non-nipped samples.

Group	Graphene weight content (%)	Average G length size (µm)	D50 (µm)	D90 (µm)	Max. (µm)	Average G agglomerate thickness (µm)
Nipped (N)	0.1	3.1±0.1	2.3	6.1	45.8	0.6±0.4
	0.5	4.0±0.1	2.5	8.5	87.1	0.7±0.2
	1.0	4.7±0.0	2.5	10.3	143.7	1.0±0.8
Non-nipped (NN)	0.1	3.2±0.0	2.4	6.3	47.5	0.5±0.4
	0.5	4.3±0.1	2.6	9.4	125.5	0.9±0.5
	1.0	4.8±0.1	2.5	10.7	123.8	1.1±0.8

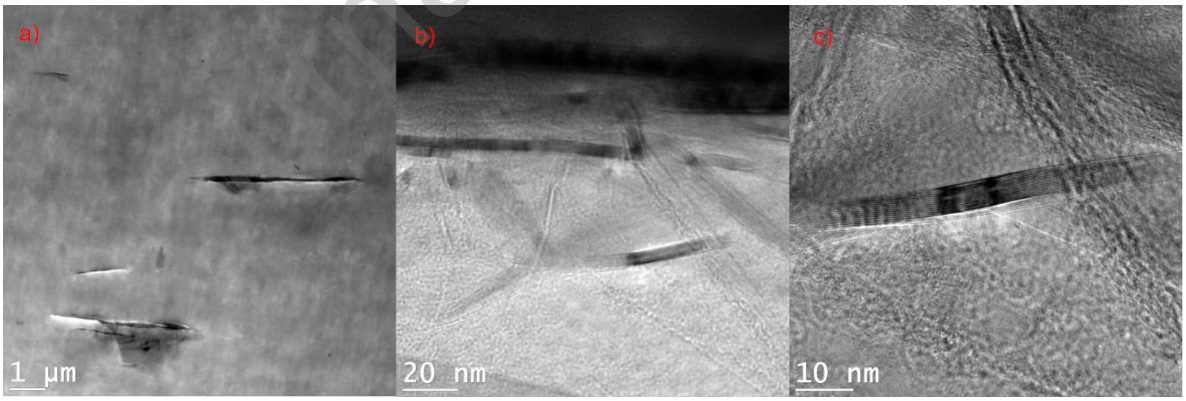

Figure 3

TEM confirms the existence of primary agglomerates as shown in Figure 3a) and suggested by OM cross section analysis, comprised by smaller particle agglomerates with few graphene layers (Figure 3c)). Thus, TEM and OM results indicate that the extrusion by SSE is inefficient to deagglomerate properly the primary agglomerates (Fig. 3b)), which therefore limits the G barrier effect as the filler content increases to

1wt.% in the nipped samples [12] as discussed in section 3.3. No great differences were found between the techniques. Furthermore, the TEM analysis indicated that the graphene agglomerates presented an average aspect ratio (AR) of 16±13.

3.3. Water and oxygen permeability performance

The use of an impenetrable phase is an important strategy to improve barrier performance in flexible packaging. In the present work, both crystalline phase of HDPE and dispersed graphene filler act as the impenetrable phases to permeating species. Table 3 shows the performance of both nipped and non-nipped HDPE/G films in terms of water and oxygen permeability and their average crystallinity.

Table 3 – Summary of water and oxygen permeability and average crystallinity percentage for nipped and non-nipped samples.

Group	Filler content (wt.%)	Water Permeability ($mg \cdot mm/m^2 \cdot day$)	Oxygen Permeability ($cm^3 \cdot mm/m^2 \cdot day$)	Average Crystallinity (%)
Nipped (N)	0	260±2	125±3	58±1
	0.1	162±6	79±1	58±2
	0.5	152±1	71±2	58±1
	1	231±2	107±2	57±1
Non-nipped (NN)	0	169±3	79±1	60±1
	0.1	156±1	73±1	59±2
	0.5	155±1	65±1	58±1
	1	151±1	67±1	59±1

Nipping the samples resulted in an increase of permeability for all films. In the case of the films without graphene this increase was more than 35% which cannot be explained by a decrease of crystallinity of the samples as the crystallinity of all samples was the same within experimental error. In any case, according to the Nielsen Model [22] (Equation 3) and considering the crystalline phase as a filler of AR equal to one [23], the decrease of permeability originating from a change of crystallinity would not be more than 13%.

$$\frac{P_C}{P_m} = \frac{1 - \varphi_S}{1 + \frac{L}{W} \cdot \frac{\varphi_S}{2}} \qquad \text{Equation 3}$$

Where the P_c/P_m ratio is the permeability ratio of the composite compared to the polymeric matrix, L/W is the aspect ratio (AR) of the barrier particle given by the length L and thickness W, and φ_s is the particle volume fraction in the composite. Therefore, the observed increase of permeability was attributed to

the presence of defects at the surface of the films induced during the surface finishing as will be discussed in the next paragraphs.

Meanwhile, G filler presented the expected effect of decreasing permeability for all samples, however, to varying extents depending on whether the films had been nipped or not. In general, for NN samples, a decrease in permeability with increasing G content was observed to a maximum of 18% with 0.5 wt.% G in oxygen permeability. As for the N samples a maximum of 43% reduction was obtained for the same G content and permeability test. But an unexpected behavior is observed at 1 wt.% G with an increase of more than 50% in permeability compared to samples with 0.5 wt.% G content.

To better understand the inconsistent results of G content and surface finishing on the permeability properties, a different layer design was used, and new films were prepared with no filler at the surface layers at both nipping and no nipping conditions. By adopting this configuration, the top and bottom layers were made only of HDPE and the inside layers were set to 1 wt.% G content. The measured oxygen permeability of the nipped and non-nipped samples were 73±1 and 72±3 $cm^3 \cdot mm/m^2 \cdot day$ corresponding to a permeability reduction of 42% and 9% compared to the neat HDPE films, respectively. Those results lead to two possible conclusions: first, the surface treatment have a dependency on the amount of filler at the surface and the permeability response is dominated by the structure developed at the surface. SEM and AFM analysis of N samples indicated the presence of surface defects such as holes and poor interface filler/polymer which possibly created preferential pathways to increase permeation. The density of defects is further increased at higher G contents, which correlates with larger agglomerations sizes (Table 2) that are expected to lead to more defects in the films (SI). Second, considering the NN samples, the presence of G at the surface is beneficial to the overall barrier ability of the films acting as a physical barrier.

The permeability experimental results were compared to the Nielsen prediction model (Eq. 3) to assess the performance of the surface finishing and the G. Figure 4 depicts experimental data and the permeability ratio as function of graphene content, assuming filler alignment perpendicular to the surface as verified by OM and TEM. Composites with particles perpendicularly aligned to the surface and with increasing AR, from 5 to 1000, were used as input in Eq.3 to plot theoretical result profiles (grey lines). The WP and OP abbreviations stand for water and oxygen permeability, respectively.

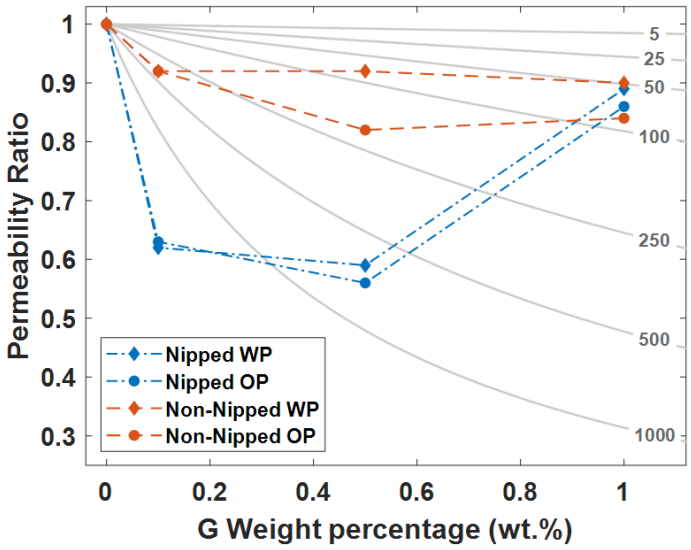

Figure 4

The model predicts a continuous permeability ratio decrease as a function of filler content for a composite with both alignment and AR fixed. Comparing the predicted results to the experimental data, G shows two behaviors depending on the sample group considered. For the NN group, a permeability reduction is obtained with G acting as a physical barrier with AR of 250-500 at 0.1 wt.% G to AR of 50-100 at 1 wt.% G which indicates that at increasing G content the deagglomeration efficiency is reduced. For the N samples, a pronounced reduction is obtained indicating that G would act as a filler with AR higher than a 1000 which is not compatible with OM and TEM analysis. Instead of having higher AR, it is possible that G hinders the influence of defects developed during surface finishing compared to the neat N sample and effectively reduces the permeability until 0.5 wt.% G. At 1 wt.% G the magnitude of reduction in permeability is hindered with increased agglomeration and reduced deagglomeration efficiency of single screw extruders at low speeds. Furthermore, the most effective barrier reduction was found for oxygen as a permeant rather than water. A smaller reduction in water permeability with the addition of G could be related to the chemical nature of HDPE itself. As HDPE is a hydrophobic material it already acts as a good barrier against water and hence, the relative difference between the neat polymer and the composites is less pronounced.

3.4. Mechanical response under tensile stress

The mechanical response of the neat and composite films was evaluated since it provides valuable data regarding the packaging material to guarantee the product integrity [24]. The main mechanical responses of the composites under tensile stress are summarized in Table 4 in the MD and TD.

Table 4 – Summary of mechanical properties of neat and composites films in the machine and transversal directions for both groups.

Group	Filler content (wt.%)	E (MPa)		Elongation at break (%) *		E ratio
		MD	TD	MD	TD (range)	
Nipped (N)	0	370±40	360±30	500	230-500	1.0
	0.1	400±30	390±30		280-500	1.0
	0.5	400±30	390±20		280-500	1.0
	1	390±30	410±50		280-490	0.9
Non-nipped (NN)	0	390±40	380±20	500	200-500	1.0
	0.1	400±30	400±20		250-500	1.0
	0.5	400±30	410±30		230-500	1.0
	1	420±20	430±20		190-360	1.0

* Elongation at break values of 500% means samples failed to break due the equipment's maximum displacement.

As the E ratio shows (MD to TD modulus ratio) no significant anisotropic response was observed. Nonetheless, the elongation at break behavior was different and is only presented for TD. Since in MD the breakage of the samples would exceed the displacement limit of the tensile equipment. This elongation behavior could be ascribed to the processing alignment of the crystalline phase experienced during processing, as supported by FTIR results (SI) and the literature [25,26].

Since it was not possible to identify a clear trend on composite's Young modulus (E) with surface finish or increasing G content, the Halpin-Tsai model [27,28] (Equation 4) was employed to evaluate and compare experimental results with the model predictions. The Halpin-Tsai model is commonly used to predict the Young's Module of a polymer composite [29]:

$$E_L = E_m\left(\frac{1+\eta_L\xi V_f}{1-\eta_L V_f}\right) \qquad \text{Equation 4}$$

The parameters η_L and ξ are defined as:

$$\eta_L = \frac{\left(\frac{E_f}{E_m}\right)-1}{\left(\frac{E_f}{E_m}\right)+\xi} \qquad \text{Equation 4.1}$$

$$\xi = \frac{2}{3}\times\frac{L}{W} \qquad \text{Equation 4.2}$$

$$E_C = E_L \qquad \text{Equation 4.3}$$

Where, the E_c, E_L, E_m and E_f are the composite, longitudinal, matrix and filler Young's moduli, respectively. V_f is the G volume fraction in the composite and L/W is the filler length L and thickness W ratio. Experimental results in MD were compared to composites containing up to 1 wt.% of G with AR ranging from 5 to 50 (TEM measurements), filler density of 2.2 g/cm^3, aligned with the processing direction, and a Young's module of 36.5 GPa that corresponds to the exfoliation between G layers [27]. The results are presented in Figure 5.

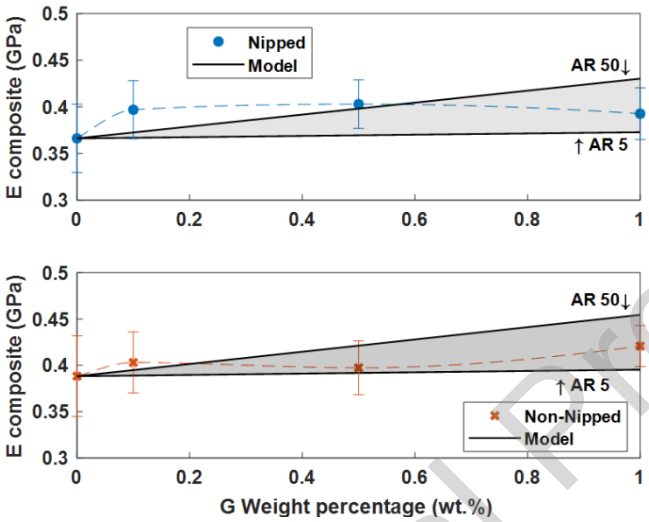

Figure 5

As shown in Figure 5, although the use of G increases the average Young's Modulus of the composites compared to the neat samples, they all fall within the experimental error which reduces the confidence of the observed effect of reinforcement. However, in general the experimental data agrees with the proposed model for both groups since the AR is reduced due to higher number of agglomerates as evidenced in the previous analyses. It is noteworthy that increased AR leads to more pronounced effects as observed by the predicted line of AR 50.

3.5. Electrical conductivity

In flexible packaging a certain level of electrical conductivity is desired to promote safe charges dissipation to protect electronics from undesired electrical discharges, for a 100 µm thick film an electrical conductivity between 10^{-06} to 10^{-11} S/cm is advised [30]. The commercial grade graphene is a conductive material. Taking this into account, the electrical conductivity was measured to evaluate if the graphene

addition at contents up to 1 wt.% would be able to cause any changes in the electrical conductivity. For the investigated filler content range, the electrical conductivity for both groups varied between 6 to 8 × 10^{-18} S/cm. So, a maximum filler concentration of 1 wt.% has no significant impact on electrical conductivity and is less than the desired range to promote safe charges dissipation. The low electrical conductivity is a result of the reduced amount of filler which is below the percolation threshold required to increase the composite conductivity. To achieve higher electrical conductivity by melt compounding, higher concentrations of filler are usually needed [31].

4. Conclusions

The effect of industrial grade graphene and surface finishing on multilayered cast HDPE films was investigated. At low filler concentration, G improved permeability properties, independently of the surface finishing. Additionally, it was also found that, although the surface finishing favors light transmittance by reducing the surface roughness of the films, the nipping process induces some defects affecting permeability. The detrimental effect of surface finishing is counteracted by layer design or the filler at concentrations lower than 1 wt.%. At this same weight concentration, the addition of graphene was not enough to cause significant difference in terms of the electrical conductivity and the barrier properties were compromised. As the theoretical model indicates this was attributed to the dispersion state of the filler, where a smaller AR resulted in decreased barrier efficiency and low mechanical reinforcement effect.

To conclude, the use of industrial grade graphene at low concentrations is attainable for industrial scale production of flexible multilayer films with improved properties. In particular, at 0.1 wt.% G a good combination of barrier properties and light transmittance was achieved through surface finishing. Nevertheless, the incorporation of 1 wt.% of graphene seems to be a limiting content at which detrimental effects on the mechanical and barrier properties were observed due to reduced dispersion efficiency. A drawback that can be partially overcome in nipped films by removing graphene from the outer layer.

Appendix A. Supplementary information

The following is the Supplementary information to this article.

Abbreviations

G
: Industrial grade graphene

MB
: Master batch

SSE
: Single screw extruders

N
: Nipped

NN
: Non-nipped

MD
: Machine direction

TD
: Transverse direction

OM
: Optical microscopy

M-T
: Machine-transverse

SR
: Surface roughness

Acknowledgements

The authors would like to acknowledge the support of the Natural Sciences and Engineering Research Council of Canada (NSERC) grant number CRDPJ 538482-18, Advanced Materials Research and Innovation Center (PRIMA) Québec grant number R-18-46, Coordenação de Aperfeiçoamento de Pessoal de Ensino Superior (CAPES), Project PROEX number 666/2016 and PRINT number 88881.310728/2018-0, Fundação de Amparo à Pesquisa e Inovação do Estado de Santa Catarina (FAPESC) number 88887.178618/2018-00, and NanoXplore. We would also like to thank the Research Center for High Performance and Composite Systems (CREPEC). And J.C.F.J. is grateful to Camila A. Zimmermann for her thoughtful comments, and the invaluable help of Claire Cerclé and Richard Silverwood from École Polytechnique Montréal, for the help with TEM and sample preparation.

References

[1] Tan B, Thomas NL. A review of the water barrier properties of polymer/clay and polymer/graphene nanocomposites. J Memb Sci 2016;514:595–612. https://doi.org/10.1016/j.memsci.2016.05.026.

[2] Jalali Dil E, Ben Dhieb F, Ajji A. Modeling the effect of nanoplatelets orientation on gas permeability of polymer nanocomposites. Polymer (Guildf) 2019;168:126–30. https://doi.org/10.1016/j.polymer.2019.02.024.

[3] Yadav SK, Jung YC, Kim JH, Ko Y-I, Ryu HJ, Yadav MK, et al. Mechanically Robust, Electrically Conductive Biocomposite Films Using Antimicrobial Chitosan-Functionalized Graphenes. Part Part Syst Charact 2013;30:721–7. https://doi.org/10.1002/ppsc.201300044.

[4] Chen JT, Fu YJ, An QF, Lo SC, Zhong YZ, Hu CC, et al. Enhancing polymer/graphene oxide gas barrier film properties by introducing new crystals. Carbon N Y 2014;75:443–51. https://doi.org/10.1016/j.carbon.2014.04.024.

[5] Sundramoorthy AK, Gunasekaran S. Applications of graphene in quality assurance and safety of food.

TrAC - Trends Anal Chem 2014;60:36–53. https://doi.org/10.1016/j.trac.2014.04.015.

[6] Kovtun A, Treossi E, Mirotta N, Scidà A, Liscio A, Christian M, et al. Benchmarking of graphene-based materials: real commercial products versus ideal graphene. 2D Mater 2019;6:025006. https://doi.org/10.1088/2053-1583/aafc6e.

[7] Kauling AP, Seefeldt AT, Pisoni DP, Pradeep RC, Bentini R, Oliveira RVB, et al. The Worldwide Graphene Flake Production. Adv Mater 2018;30:1803784. https://doi.org/10.1002/adma.201803784.

[8] Mohan VB, Lau K tak, Hui D, Bhattacharyya D. Graphene-based materials and their composites: A review on production, applications and product limitations. Compos Part B Eng 2018;142:200–20. https://doi.org/10.1016/j.compositesb.2018.01.013.

[9] Kalaitzidou K, Fukushima H, Drzal LT. Multifunctional polypropylene composites produced by incorporation of exfoliated graphite nanoplatelets. Carbon N Y 2007;45:1446–52. https://doi.org/10.1016/j.carbon.2007.03.029.

[10] Boldt R, Leuteritz A, Schob D, Ziegenhorn M, Wagenknecht U. Barrier Properties of GnP–PA-Extruded Films. Polymers (Basel) 2020;12:669. https://doi.org/10.3390/polym12030669.

[11] Oyarzabal A, Cristiano-Tassi A, Laredo E, Newman D, Bello A, Etxeberría A, et al. Dielectric, mechanical and transport properties of bisphenol A polycarbonate/graphene nanocomposites prepared by melt blending. J Appl Polym Sci 2017;134. https://doi.org/10.1002/app.44654.

[12] Jin J, Rafiq R, Gill YQ, Song M. Preparation and characterization of high performance of graphene/nylon nanocomposites. Eur Polym J 2013;49:2617–26. https://doi.org/10.1016/j.eurpolymj.2013.06.004.

[13] Morris BA. Introduction. Sci. Technol. Flex. Packag., Elsevier; 2017, p. 3–21. https://doi.org/10.1016/B978-0-323-24273-8.00001-0.

[14] McNally GM, Small CM, Murphy WR, Garrett G. The Effect of Polymer Properties on the Mechanical Behavior and Morphological Characteristics of Cast Polyethylene Film for Stretch and Cling Film Applications. J Plast Film Sheeting 2005;21:39–54. https://doi.org/10.1177/8756087905052804.

[15] Madinehei M, Kuester S, Kaydanova T, Moghimian N, David É. Influence of Graphene Nanoplatelet Lateral Size on the Electrical Conductivity and Electromagnetic Interference Shielding Performance of Polyester Nanocomposites. Polymers (Basel) 2021;13:2567. https://doi.org/10.3390/polym13152567.

[16] Moghimian N, Nazarpour S. The Future of Carbon: An Update on Graphene's Dermal, Inhalation, and Gene Toxicity. Crystals 2020;10:718. https://doi.org/10.3390/cryst10090718.

[17] NanoXplore. GrapheneBlack 3X Technical Data Sheet 2021:3.

[18] Duffo P, Monasse B, Haudin JM. Influence of Stretching and Cooling Conditions in Cast Film Extrusion of PP Films. Int Polym Process 1990;5:272–83. https://doi.org/10.3139/217.900272.

[19] Ehrenstein GW, Riedel G, Trawiel P. Differential Scanning Calorimetry (DSC). Therm. Anal. Plast. - Theory Pract., Hanser Publishers; 2004, p. 15.

[20] Marini J, Bretas RES. Optical Properties of Blown Films of PA6/MMT Nanocomposites. Mater Res 2017;20:53–60. https://doi.org/10.1590/1980-5373-mr-2017-0280.

[21] Palomba M, Longo A, Carotenuto G, Coscia U, Ambrosone G, Rusciano G, et al. Optical and electrical characterizations of graphene nanoplatelet coatings on low density polyethylene. J Vac Sci Technol B, Nanotechnol Microelectron Mater Process Meas Phenom 2018;36:01A104.

https://doi.org/10.1116/1.4998570.

[22] Nielsen LE. Models for the Permeability of Filled Polymer Systems. J Macromol Sci Part A - Chem 1967;1:929–42. https://doi.org/10.1080/10601326708053745.

[23] Duan Z, Thomas NL. Water vapour permeability of poly(lactic acid): Crystallinity and the tortuous path model. J Appl Phys 2014;115:064903. https://doi.org/10.1063/1.4865168.

[24] Morris BA. Strength, Stiffness, and Abuse Resistance. Sci. Technol. Flex. Packag. - Multilayer Film. from Resin Process to End Use, Elsevier; 2017, p. 309.

[25] Yadegari A, Morshedian J, Khonakdar H-A, Wagenknecht U. Influence of annealing on anisotropic crystalline structure of HDPE cast films. Polyolefins J 2016;3:1–9.

[26] Fatahi S, Ajji A, Lafleur PG. Correlation between Structural Parameters and Property of PE Blown Films. J Plast Film Sheeting 2005;21:281–305. https://doi.org/10.1177/8756087905059979.

[27] King JA, Klimek DR, Miskioglu I, Odegard GM. Mechanical properties of graphene nanoplatelet/epoxy composites. J Compos Mater 2015;49:659–68. https://doi.org/10.1177/0021998314522674.

[28] Dul S, Fambri L, Merlini C, Barra GMO, Bersani M, Vanzetti L, et al. Effect of graphene nanoplatelets structure on the properties of acrylonitrile–butadiene–styrene composites. Polym Compos 2019;40. https://doi.org/10.1002/pc.24645.

[29] Shokrieh MM, Moshrefzadeh-Sani H. On the constant parameters of Halpin-Tsai equation. Polymer (Guildf) 2016;106:14–20. https://doi.org/10.1016/j.polymer.2016.10.049.

[30] Tolinski M. 6.1.3 Conductive Fillers as Antistatic/ESD Additives. Addit. Polyolefins - Get. Most Out Polypropylene, Polyethyl. TPO. 2nd ed., Elsevier; 2015, p. 62.

[31] Batista NL, Helal E, Kurusu RS, Moghimian N, David E, Demarquette NR, et al. Mass-produced graphene—HDPE nanocomposites: Thermal, rheological, electrical, and mechanical properties. Polym Eng Sci 2019;59:675–82. https://doi.org/10.1002/pen.24981.

Figures captions

Figure 1 – Percentage of transmitted light in 500 nm as function of surface roughness for nipped and non-nipped samples.

Figure 2 – The top row presents top view pictures of a) NN 0.1 wt.% G, b) NN 0.5 wt.% G and c) NN 1 wt.% G. The bottom row presents cross section pictures of d) NN 0.1 wt.% G, e) NN 0.5 wt.% G and f) NN 1 wt.% G.

Figure 3 – TEM in the M-T plane showing a) primary agglomerates, b) non-exfoliated graphene and c) Few layers of graphene in the 0.5 wt.% NN composite.

Figure 4 – Permeability ratio as function of filler weight concentration for experimental and predicted data. The lines between the experimental data points are just a guide to the eyes. The indicated numbers in the grey lines are the used AR.

Figure 5 – Young's modulus of composites and model with AR between 5 and 50 for nipped and non-nipped samples.

CRediT authorship contribution statement

José Carlos Ferreira Junior: Conceptualization, Methodology, Software, Investigation, Writing - Original Draft. Nima Moghimian: Writing - Review & Editing. Giovanna Gutiérrez: Writing - Review & Editing. Helal, Emna: Writing - Review & Editing. Abdellah Ajji: Supervision, Writing - Review & Editing. Guilherme Mariz de Oliveira Barra: Supervision, Writing - Review & Editing. Nicole R Demarquette: Project administration, Funding acquisition, Supervision, Writing - Review & Editing.

Declaration of interests

☐ The authors declare that they have no known competing financial interests or personal relationships that could have appeared to influence the work reported in this paper.

☒The authors declare the following financial interests/personal relationships which may be considered as potential competing interests:

The authors have received a partial funding from Nanoxplore or are employees and/or shareholders of NanoXplore Inc.

Graphical abstract

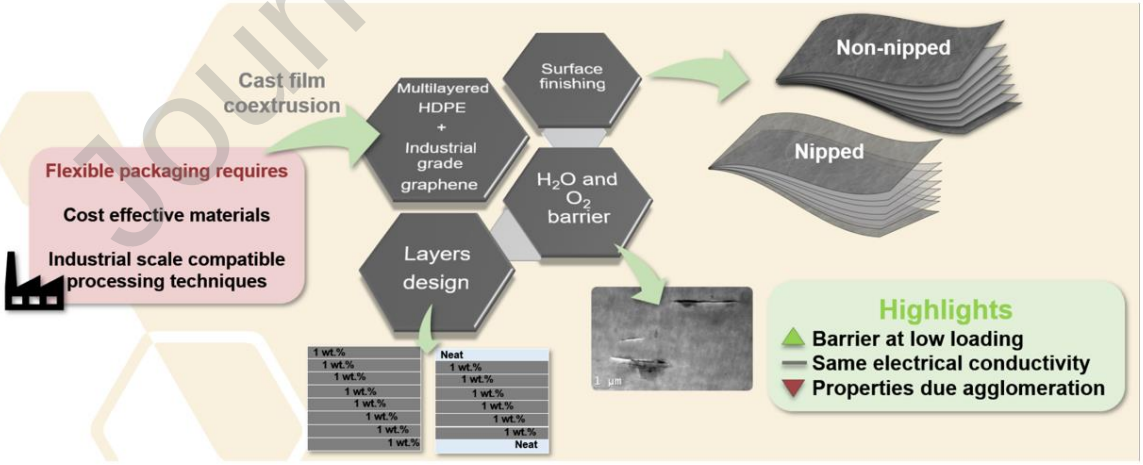

Highlights

- Industrial grade graphene can be used for flexible packaging applications.
- 0.5 wt.% of industrial grade graphene reduced the oxygen permeability in 43%.
- Layer design allows to overcome filler dispersion shortcomings.